Carderock Division, Naval Surface Warfare Center
West Bethesda, Maryland 20817-5700

NSWCCD-50-TR-2007/009 May 2007

Hydromechanics Department Report

Velocity Measurements Through the Pump of the X-Craft Tow Tank Model 5612

by

Christopher J. Chesnakas

REPORT DOCUMENTATION PAGE

Form Approved
OMB No. 0704-0188

1. REPORT DATE *(DD-MM-YYYY)*	2. REPORT TYPE	3. DATES COVERED *(From - To)*
May 2007	Technical	June - October 2006

4. TITLE AND SUBTITLE
Velocity Measurements Through the Pump of the X-Craft Tow Tank Model 5612

5a. CONTRACT NUMBER

5b. GRANT NUMBER

5c. PROGRAM ELEMENT NUMBER

6. AUTHOR(S)
Christopher J. Chesnakas

5d. PROJECT NUMBER

5e. TASK NUMBER

5f. WORK UNIT NUMBER
06-1-2123-404

7. PERFORMING ORGANIZATION NAME(S) AND ADDRESS(ES) AND ADDRESS(ES)

Naval Surface Warfare Center
Carderock Division
9500 Macarthur Boulevard
West Bethesda, MD 20817-5700

8. PERFORMING ORGANIZATION REPORT NUMBER

NSWCCD-50-TR-2007/009

9. SPONSORING / MONITORING AGENCY NAME(S) AND ADDRESS(ES)

10. SPONSOR/MONITOR'S ACRONYM(S)
NAVSEA PMS 325

11. SPONSOR/MONITOR'S REPORT NUMBER(S)

12. DISTRIBUTION / AVAILABILITY STATEMENT
Approved for public release. Distribution unlimited.

13. SUPPLEMENTARY NOTES

14. ABSTRACT

Flow through the pumps on a 1/15th scale model of the X-Craft, Model 5612, was measured. An external, strut-mounted, three-component LDV system was used to measure the flow ahead of the pump inlet, and an internal, three-component LDV system was used to measure the flow ahead of the rotor and inside the nozzle of the waterjet. These tests revealed the flow structure within the pump, and allowed the calculation of terms required for an analysis of the pump performance. The pump was tested at two underway speeds corresponding to 25 and 40 knots full scale and at two bollard conditions.

15. SUBJECT TERMS
Waterjet, LDV, Propulsion

16. SECURITY CLASSIFICATION OF:			17. LIMITATION OF ABSTRACT	18. NUMBER OF PAGES	19a. NAME OF RESPONSIBLE PERSON
a. REPORT	b. ABSTRACT	c. THIS PAGE			Christopher Chesnakas
UNCLASSIFIED	UNCLASSIFIED	UNCLASSIFIED	Unlimited	31	19b. TELEPHONE NUMBER *(include area code)* (301) 227-5833

(THIS PAGE INTENTIONALLY LEFT BLANK)

CONTENTS

FIGURES

TABLES

SYMBOLS

D_i	Diameter of the inlet, 3.281 inches
D_r	Diameter of the rotor, 4.234 inches
L	Length of hull at waterline, 191.88 inches
Q	Volume flow rate
q	Root-mean-square (RMS) fluctuation of velocity, TKE = $\rho q^2/2$, normalized by U_∞
u	Root-mean-square (RMS) fluctuation of axial velocity component
U_r	Velocity radially outward from shaft axis, normalized by U_∞
U_{ref}	Rotor reference velocity, $\pi \cdot D_i \cdot$rpm/60
U_t	Velocity tangential to shaft axis, normalized by U_∞
U_x	Velocity in direction of model axis, normalized by U_∞ (+ downstream)
U_y	Velocity in horizontal direction, perpendicular to model axis, normalized by U_∞ (+ starboard)
U_z	Velocity in vertical direction, normalized by U_∞ (+ up)
U_∞	Model speed
x	Coordinate along hull axis, from bow waterline, normalized by L
y	Coordinate in transverse direction, normalized by L (+ starboard)
z	Coordinate vertical direction, normalized by L (+ up)
β_E	Energy non-uniformity coefficient, see Equation 9
β_M	Momentum non-uniformity coefficient, see Equation 8
θ_2	Angle between measured velocity component 2 and z axis
θ_3	Angle between measured velocity component 3 and z axis

(THIS PAGE INTENTIONALLY LEFT BLANK)

ABSTRACT

Flow through the pumps on a 1/15th scale model of the X-Craft, Model 5612, was measured. An external, strut-mounted, three-component LDV system was used to measure the flow ahead of the pump inlet, and an internal, three-component LDV system was used to measure the flow ahead of the rotor and inside the nozzle of the waterjet. These tests revealed the flow structure within the pump, and allowed the calculation of terms required for an analysis of the pump performance. The pump was tested at two underway speeds corresponding to 25 and 40 knots full scale and at two bollard conditions.

ADMINISTRATIVE INFORMATION

This work was sponsored by the Naval Sea Systems Command (NAVSEA) PMS 325 Sealift R&D Program, Task Line - High Speed Sealift; and was performed jointly by the Propulsion and Fluid Systems Division (Code 5400) and the Resistance and Powering Division (Code 5200) of the Hydromechanics Department, NSWC Carderock Division, West Bethesda, Maryland. The work was performed between June and October 2006 using the Work Unit Number 06-1-2123-404.

EXPERIMENTAL APPARATUS

Model

The hull used in the test, Model 5612, is a 1/15 scale model of FSF-1 *Sea Fighter* (X-Craft). The Model is a catamaran, 191.88 inches (4874 mm) long at the waterline. The hull is powered by 4 waterjets, 2 in each side hull. The model waterjets are AWJ-21 units, manufactured at NSWCCD. These pumps, shown in cutaway in Fig. 1, are not the same as on *Sea Fighter*, which has KaMeWa pumps. Geometry for the pumps on Sea Fighter was not available, so the AWJ-21 pumps were used as surrogates. The geometry of the inlet and the nozzle, however, matches the full-scale hull.

T-foils were mounted on each side hull at $x/L = 0.177$ as shown in Fig. 2. The foils had an 8 inch (203 mm, $0.0417 \cdot L$) span and were mounted 2.25 inches (57 mm) below the hull. For this test, the foils were fixed with an angle of 1° down with respect to the nominal waterline.

LDV System

The LDV measurements were made using two different LDV systems — an external and an internal system. The external system was used for measurements ahead of the inlet at station 1, and the internal system was used for measurements just ahead of the rotor, station 3, and at the nozzle exit, station 6. The locations of the stations are shown in Fig. 1. The common components of the two systems will first be described, and then the specific components of the two systems will be explored.

Base System

Doppler signals were analyzed with a TSI Model IFA 655 Digital Burst Correlator. The processor performs a 256-sample, double-clipped, autocorrelation on each doppler burst, allowing the measurement of velocity even when the signal-to-noise ratio is low. In order to maximize data rate, the processors were operated in the random mode. The processors were linked to a motor controller, which automated the stepping of the probes through the measurement grid during runs down the basin.

The flow about the hull was seeded with 1500-grit silicon carbide powder, 1 to 2μm in size. The powder was mixed into a slurry with water and injected through nine 0.1-inch diameter taps in the hull at $x/L = 0.24$.

External LDV System

The external LDV system consisted of two TSI Model 9832, 83mm (3.25 inch) diameter, fiber-optic probes attached to each other on a streamlined strut as shown in Figs. 3 and 4. The probes were mounted rigidly together on the strut in order to keep the measurement volumes aligned. In order to measure at different points in the flow, the probes could be translated in a plane perpendicular to the model axis as a unit.

The upper probe in Fig. 3 used the green (514.5 nm) and blue (488 nm) beams of an argon-ion laser to measure two components of velocity , U_1 and U_2, and the lower probe used the violet (476.5 nm) beams of the laser to measure a third component, U_3. The probes are oriented with their axes parallel to the flow direction (the x axis), and have prisms at the front lens to deflect the beams by 90°. The probes have 50 mm beam spacing and 500mm focal length (air) lenses. Each probe has an elliptical probe volume with a major axis of 2.0 mm and both minor axes of 0.01 mm. The probe volumes are approximately 620 mm from the probe centerlines in water.

The fringe spacing for the green, blue, and violet beams was 5.266μm, 4.991μm, and 4.872μm, respectively. The probes were oriented so that the green channel measured the axial component of velocity, U_1, the blue channel measured a velocity component U_2 perpendicular to the x axis and at 19.90° to the z axis, and the violet channel measured a velocity component U_3 perpendicular to the x axis and at 63.60° to the z axis. These angles were designed to give maximum access to the flowfield while keeping the strut and probes as far from the model as possible. The relative distance from the strut to the hull is illustrated in Figs. 5 and 6.

The strut consisted of 2 × 4 inch (51 × 102 mm) aluminum extrusions bolted together in an L shape. On the leading and trailing edges of the strut, 4-inch long double-circular-arc fairings of renshape were attached. These fairings had interior passages to pass the probe cables. A 6 × 0.72 inch (152 × 18.3 mm) streamlined brace was attached at a 45° angle between the two legs of the strut to provide extra rigidity.

The strut assembly was attached to the carriage through a two-component, computer controlled traverse. The traverse sat on the carriage, above the water level. The traverse was powered by two stepper motors attached to 5-thread-per-inch lead screws. Position was determined by rotary encoders mounted to the stepper motors.

The traverse could move the probes in the y and z directions. Positioning in the x direction was achieved by manually moving the hull on the center rail of the carriage. The range of movement in the y direction was approximately 19 inches (480 mm), and the in the z direction the measurement volume could be positioned to approximately 20 inches (510 mm) below the water surface.

Internal LDV System

The internal LDV system consisted of two TSI Model 9812, 25mm (1 inch) diameter, fiber-optic probes mounted together as shown in Fig. 7. The probes were mounted at 50° to one another, with the two probe volumes aligned to be coincident. The first probe transmitted the green and blue beams through a 135mm focal length (air) lens and the second probe transmitted the violet beams through a 102mm focal length (air) lens.

In order to make measurements inside the pump, two 0.7-inch wide slots covering 220° of arc were cut into the inboard starboard pump housing to allow optical access to the LDV probes. These slots were just ahead of the rotor at $x/L = 0.984$, and in the nozzle at $x/L = 1.021$. At these locations, the inside diameters of the pump were 3.281" and 2.034" (83.34 mm and 51.66 mm) , respectively. In each slot was a thin (0.030"), curved polycarbonate windows bonded to a stereo-lithography-produced resin frame that held the window flush with the inner surface. The windows prevented flow through the slots and ensured that the flow remained undisturbed. Surrounding each window was a tank which kept the probes immersed in water. In this way, as the probes traversed to various points in the flowfield, the optical path length remained equal, and the probe volumes remained aligned. The water tank at station 6 can be seen in Figs. 9 and 10.

At the aft measurement station, station 6, the probe assembly was mounted with the probes each at 25° to the vertical (z) axis as shown in Figs. 8 and 9. At station 6, the inboard (port) probe used the blue (488nm) output of an argon-ion laser to measure velocity in the x-direction and the green (514.5nm) output to measure velocity in the y-z plane at 205° to the y axis. The outboard probe used the violet (476nm) output of the argon-ion laser to measure a component of velocity in the y-z plane at 155° to the y axis. The fringe spacing for the green, blue, and violet beams was 4.951μm, 4.788μm, and 3.517μm, respectively.

At the forward measurement station, station 3, the probe assembly was mounted with the first probe at 10° to the vertical (z) axis and the second probe at 40° to the z axis as shown in Fig. 11. The inboard probe used the blue (488nm) output to measure velocity in the x-direction, and the outboard probe used the violet (476nm)

output of the argon-ion laser to measure velocity in the x-direction as well. This was done to minimize the regions of the flow which could not be measured. As shown in Fig. 12, the hub at station 3 blocks a considerable portion of the flow from being measured by each probe. The region blocked from being measured by both probes, however, is fairly small. With the arrangement used, the axial component of velocity is measured over most of station 3, instead of measuring all three components of velocity over a considerably smaller portion of station 3.

PROCEDURE

Test Conditions

All tests were performed on carriage 2 of the David Taylor Model Basin. The model was tested in the underway condition at 6.45 and 10.33 knots, corresponding to full-scale speeds of 25 and 40 knots. The model was fixed in heave and trim at the neutral self-propelled values (determined in an earlier phase of testing) for each speed. Waterjet speeds for the modeled self-propulsion points were determined in previous experiments assuming the standard tow force augment to offset the excess viscous drag due to the Reynolds Number disparity.

Table 1. Test conditions.

Condition	Hull Speed (kt.)		*Fn*	Rotor Speed	Sinkage	Hull Pitch
	Model	Full		rpm	(in.)	(deg.)
Underway	6.45	25	0.48	1784	0.91	+1.37
Underway	10.33	40	0.77	2350	0.36	+0.64
Bollard	0		0	1500	0	0
Bollard	0		0	2500	0	0

The measurements were also performed in a bollard condition (hull stationary in the water) to verify the waterjet flow rate calibration performed by conventional means. Data were collected with the pumps running at 1500 rpm and 2500 rpm. Measurements were taken well away from obstacles in the basin so that there would be minimal interference. No blocking board was used. The run conditions are listed in Table 1.

Measurements were made at station 3 (rotor inlet, x/L = 0.984) only at the 25 kt. underway condition. Measurements were made at station 1 (ahead of inlet, x/L = 0.862) at both the 25 kt. and 40 kt. underway conditions. Measurements were made at station 6 (nozzle, x/L = 1.021) at all test conditions.

Data Acquisition

Measurements were made only on the starboard hull. At station 1, measurements were made across the hull, in front of both inlets. At stations 3 and 6, measurements were made only on the inboard starboard pump.

Before data were acquired, it was first necessary to establish the position of the LDV measurement volume. This was done by using reference marks. At station 1 a mark was placed on the side of the hull below the waterline. At stations 3 and 6, a glass reticle with an etched crosshair was paced in a socket above the pump. Alignment on the mark could be viewed through the clear plexiglas water tank, and the reticle was removed for measurements in the pump.

At each axial location, a grid of points in the flow was measured. At station 1 the grid came to 0.10 inches from the wall, and at stations 3 and 6, the grid came to 0.06 inches from the wall. During each carriage pass, the probe assembly was moved to different positions under computer control. Between 15 and 36 points could be obtained in each pass, depending on the model speed and data rate; lower towing speeds allowed longer runs, and thus more time for data collection.

At each measurement point in the flow, data were acquired for either 2 seconds or 20000 velocity realizations, whichever came first. Since the signal-to-noise ratio and the seeding density varied through the flow, the actual number of measurements at each point in space varied. Data rates reached as high as 3000 samples per second on each channel, but could be substantially lower near the wall. Data rate was generally nearly equal for the three components, but near the wall this could change.

Data Reduction

Velocity Components

Three components of velocity, U_1, U_2, and U_3, were measured at stations 1 and 6 with the present system, but the components were not aligned with the x, y, and z axes of the model, nor were they perpendicular. The measured velocities are transformed to the model coordinates by

$$U_x = U_1 \tag{1}$$

$$U_y = \frac{-U_2 \cos\theta_3 + U_3 \cos\theta_2}{\sin(\theta_3 - \theta_2)} \tag{2}$$

$$U_z = \frac{U_2 \sin\theta_3 - U_3 \sin\theta_2}{\sin(\theta_3 - \theta_2)} \tag{3}$$

where θ_2 and θ_3 are the angles between the second and third measured velocity components and the vertical (z) direction. At station 1 $\theta_2 = 19.9°$, and $\theta_3 = 63.6°$. At station 6 $\theta_2 = 205.0°$, and $\theta_3 = 155.0°$. The rms velocity, q, is calculated at stations 3 & 6 by taking the square root of the sum of the variances in velocity of the three measured components.

At station 3, only the axial component of velocity was measured, so no transformations were needed. At locations where both probes measured the velocity, the reported velocity is the average of the two measurements. The rms of the axial velocity, u, is calculated at station 3 by taking:

- the square root of the variance in velocity if only one probe measured the velocity
- the square root of 0.5 times the sum of the variances in velocity if two probes measured the velocity.

Strut Interference Corrections

Although the measurement volume was some distance from the probes and strut, there was still some disturbance of the measured flow by the hardware at station 1. This disturbance is the result of flow being deflected by the probes and strut, and from waves generated by the probes and strut. Due to the free surface, the effect is a function both of carriage speed and measurement depth. The disturbance was quantified by measuring the water velocity at various depths with no model attached. If there is no disturbance of the flow, U_1 should measure the carriage speed, and U_2 and U_3 should be zero. A correction to bring the no-model velocities to their ideal values was calculated. The corrections are:

$$U_{x\,corrected} = \frac{U_{x\,raw}}{0.994} \tag{4}$$

$$U_{y\,corrected} = U_{y\,raw} + U_{x\,corrected}\left(-0.009 - z \cdot 2.6 \times 10^{-5}\right) \tag{5}$$

$$U_{z\,corrected} = U_{z\,raw} + U_{x\,corrected}\left(0.001 - z^2 \cdot 3.6 \times 10^{-5}\right) \tag{6}$$

where z is the distance below the undisturbed water surface, in inches, and the velocities are normalized by model speed. The resultant corrections are small — generally less than 1% of model speed. These corrections are applied to the measurements at station 1. No corrections were needed at stations 3 & 6, since no LDV hardware was in the flow.

Integrated Flux Coefficients

The velocity measurements can be integrated to obtain coefficients used in the calculation of the waterjet performance. To do this, the velocity measurements must first be interpolated to the wall. Grid points were added to the measurement set at the wall with axial velocity equal to C times the velocity at the nearest measured point to approximate the momentum of a turbulent boundary layer. The factor C was set to 0.8 at station 3 and 0.85 at station 6, where the boundary layer was thinner. The wall radial and tangential velocities were set to zero. For the points at station 3 in the hub shadow, velocities were interpolated from nearby measurements.

At each station, the flow rate, Q, was calculated by numerically integrating across the flow area

$$Q = \int U_x dA \tag{7}$$

Note that the integration area is perpendicular to the x-direction. The average velocity at each measurement plane, $\overline{U}$, is then Q/A.

The momentum and energy non-uniformity factors were calculated at each station by integrating

$$\beta_M = \frac{1}{A}\int\left(\frac{U_x}{\overline{U}}\right)^2 dA \tag{8}$$

$$\beta_E = \frac{1}{A}\int\frac{U_x(U_x^2+U_y^2+U_z^2)}{\overline{U}^3} dA \tag{9}$$

Additionally, the energy non-uniformity factor could be divided into three parts, β_{Ex}, β_{Et}, and β_{Er}, to show the relative kinetic energy contributions from the axial, tangential, and radial (relative to the pump axis) velocity components. These terms are defined as

$$\beta_{Ex} = \frac{1}{A}\int\frac{U_x^3}{\overline{U}^3} dA \qquad \beta_{Et} = \frac{1}{A}\int\frac{U_x U_t^2}{\overline{U}^3} dA \qquad \beta_{Er} = \frac{1}{A}\int\frac{U_x U_r^2}{\overline{U}^3} dA \tag{10}$$

EXPERIMENTAL RESULTS

Velocity Planes

Measurements were obtained on a grid of 399 points at station 1 and 361 points at stations 3 & 6. At these planes, plots are shown with color contours of the velocity component in the direction of the model axis, U_x, and of the rms of the velocity fluctuations, q. Note that $\rho q^2/2$ is equal to the turbulent kinetic energy. For the plots at stations 1 & 6, vectors of the in-plane velocities, looking upstream are plotted on top of the color contours. In all plots, distances are normalized by the ship length, L. In the plots of the underway flowfield, velocities are normalized by the ship speed, U_∞, and in the plots of the bollard flowfield, velocities are normalized by the reference rotor speed, $U_{ref} = \pi \cdot D_i \cdot$rpm/60. The magnitudes of the plotted velocities at the bollard condition differ from those on the underway flow by about a factor of two. This is the approximate ratio of reference rotor speed to hull speed for the underway conditions, as shown in Table 2.

Plots of the velocity ahead of the inlet at station 1 are shown in Figs. 13 - 16. In these figures, the position of the hull and the pump inlets are shown by the black lines. Also shown in Fig. 13 is the projection of the T-foil location. The $y = 0$ location is at the model centerline, and the $z = 0$ location is at the model baseline (lowest point of the hull). The measurements are located at the tail of each of the plotted vectors. The boundary

layer ahead of the inlets is not uniform. The interaction of suction from the pumps, cross flow on the hull, surface wave effects, and the T-foil wake causes the boundary layer thickness to vary considerably. The effects of surface waves and cross flow are particularly strong at the 25 knot condition. A vortex is seen at the inboard side of the hull, which is hypothesized to be from interactions with (or waves from) the port hull.

Table 2. Hull and rotor speeds.

Hull Speed		Rotor Speed	Reference Rotor Speed, U_{ref}	U_{ref}/Hull Speed
Full (kt.)	Model (ft/s)	rpm	$\pi \cdot D_i \cdot$rpm/60 (ft/s)	
25	10.90	1784	25.54	2.34
40	17.43	2350	33.64	1.93
0	0	1500	21.47	∞
0	0	2500	35.79	∞

Plots of the flow in the inlet at station 3 are shown in Figs. 17 – 18. In these figures the position of the pump wall and hub are shown by the outer and inner black circles, respectively and the $y = z = 0$ location is at the shaftline. It was not possible to measure all the way to the hub or the wall due to light reflection off of the solid surfaces. Also, both plots show a region below and to the right of the shaft which has no data. This is the region of the flow shadowed by the hub, as explained in the *Experimental Apparatus – LDV System – Internal LDV System* section. The measurement grid for station 3 is shown on top of the velocity fluctuation contours of Fig. 18.

The axial velocity at station 3, Fig. 17, shows a large gradient from the top to the bottom of the rotor disk. Even though only a single component of velocity was measured at this station, it is apparent that there is swirl in the inflow. The shaft wake, seen as the region of low velocity and high turbulence above the hub in the two figures, is clearly skewed in the direction of the rotor rotation. The rotor rotation is being felt upstream, most likely through the shaft boundary layer.

Plots of the mean flow underway at station 6 are shown in Figs. 19 - 22. The plots show a swirl over most of the flow in the direction of the rotor rotation, and reversed swirl in the hub wake. The two conditions look very similar except for the velocity magnitude. The non-dimensional velocity at station 6 is significantly higher at 25 knots than for 40 knots. This is presumed to be caused by the resistance characteristics of the hull. The resistance curve has a hump at 25 knots, and since the model was run in self propulsion, the pumps have to provide relatively more thrust at this speed.

The plots of the mean flow at the two bollard conditions are shown in Figs. 23 and 24. Note that in these figures the missing data was caused by a crack which appeared in the polycarbonate window which blocked one of the beams along a line of points. This data along this line was corrected before integrations were performed. The swirl pattern in the bollard plots is very similar to that seen in the underway plots, but the distribution of the

axial velocity is different. In the underway condition, the lowest velocity was at the top of the flowfield, in the bollard condition, the lowest velocity has rotated to the outboard side.

Integrated Flux Coefficients

The velocity fields were extrapolated to the walls and integrated, as explained in the *Procedure – Data Reduction* section, to obtain the average velocity and flow rate, and the momentum and energy non-uniformity coefficients. The flowfields used for the integrations are shown in Figs. 25 – 31. The integration areas are naturally bounded at stations 3 and 6 by the walls of the pump, but the flow area is not so easily defined at station 1. For station 1, the flow area was chosen by:

1. Centering the inlet flow area in front of the pump. The angle of the flow at station 1 varied throughout the flowfield, making an offset for the flow area difficult to determine. Due to the relatively small gradients across the flowfield in the y direction, this should not greatly affect the integrated results.
2. Choosing a "half football" shape for the inflow area approximately 1.5 times the inlet diameter in width. Several studies on other hulls have shown this to be the correct shape for the inflow area to a waterjet.
3. Adjusting the edges of the inflow area so that the mass flow through station 1 matches that calculated at stations 3 and 6.

Table 3. Integrated flux coefficients, inboard starboard pump, underway.

Station	Term	Magnitude		Multiplier
		25 kt.	40 kt.	
1	U_{avg}	0.907	0.892	U_∞
1 *outbd*		*0.908*	*0.914*	
3		0.788		
6		2.002	1.679	
3	Q	1.741E-04		$U_\infty L^2$
6		1.764E-04	1.480E-04	
1	β_M	1.009	1.007	
1 *outbd*		*1.010*	*1.007*	
3		1.026		
6		1.002	1.002	
1	β_{Ex}	1.024	1.019	
1 *outbd*		*1.028*	*1.018*	
3		1.076		
6		1.006	1.006	
6	β_{Et}	0.014	0.013	
6	β_{Er}	0.001	0.001	
1	β_E	1.030	1.022	
1 *outbd*		*1.031*	*1.020*	
6		1.022	1.020	

quantities calculated for the outboard starboard pump in italics

The flow areas thus chosen for station 1 are shown in Figs. 28 and 29. It should be noted that the inflow area is smaller at 40 knots than at 25 knots. This is due to the higher resistance of the hull, and thus higher flow through the pump, at 25 knots.

The results of these integrations are listed in Tables 3 and 4. The flow rate at 25 kt was found both at station 3 and at station 6. The flow rate calculated at these two stations differs by 1.3%. Since the accuracy of the flow rate measurement is 2.8%, the measurements agree within the expected tolerance. Most of the measurements in this test were on the starboard inside pump. The measurements at station 1, however, covered the inflow into both the starboard inboard and outboard pumps. Quantities calculated for the outboard pump are printed in red in Table 3. For most calculated terms, there is little difference between the inboard and outboard pumps. The average velocity entering the pump is significantly higher on the outboard pump at 40 knots than on the inboard. This result should be compared to the pressure and dynamometer measurements at these conditions. The actual flow rates at each condition are compared in Table 5.

Although the non-uniformity in the flow appears to be large in the plots of the velocity fields, the integrated flow coefficients show the non-uniformity to be similar to, or less than previously-measured waterjet-powered monohulls. For example, on this model β_{Ex3} was found to be 1.076, and β_{E6} was around 1.02. Measurements on the Gulf Coast waterjet model[1], found β_{Ex3} to be 1.058 and β_{E6} to be 1.06, while measurements on Model 5565-1[2, 3] found β_{Ex3} to be 1.25 and β_{E6} to be 1.06.

Table 4. Integrated flux coefficients, inboard starboard pump, bollard.

Term	Magnitude		Multiplier
	1500 rpm	2500 rpm	
U_{avg}	0.764	0.762	U_{ref}
Q	6.74E-05	6.72E-05	$U_{ref}L^2$
β_M	1.002	1.003	
β_{Ex}	1.006	1.008	
β_{Et}	0.030	0.028	
β_{Er}	0.002	0.001	
β_E	1.039	1.037	

Table 5. Volume flux at station 6, ft^3/s.

Condition	Q (ft^3/s)
25 kt. (1784 rpm)	0.491
40 kt. (2350 rpm)	0.660
1500 rpm bollard	0.370
2500 rpm bollard	0.614

SUMMARY AND CONCLUSIONS

Measurements of the flow through the inboard starboard pump on the X-Craft tow-tank model, Model 5612, document the flow through the pumps. The measurements show significant non-uniformity of the flow entering the pumps. The interaction of cross flow on the hull, surface wave effects, suction from the pumps, and the T-foil wake causes the hull wake at station 1 to depart significantly from a 2-D boundary layer. The jet velocity ratio was found to be much higher at 25 knots than at 40 knots due to the increase in hull resistance near the 25 knot speed. Non-uniformity of the flow inside the pump at stations 3 and 6 was found to be similar to, or less than that found on previously measured waterjet models.

ACKNOWLEDGEMENTS

Model setup, rigging, and operation was performed by Bryson Metcalf of Code 5200.

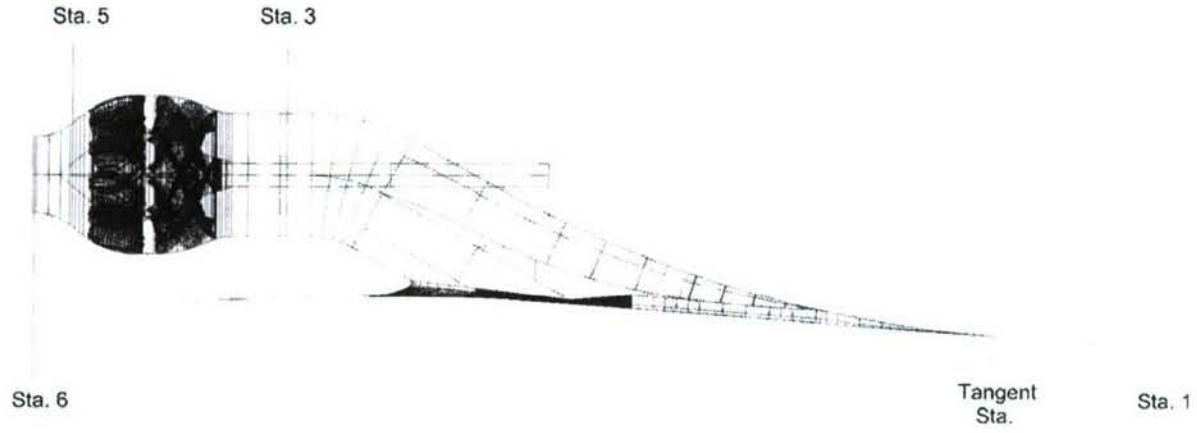

Fig. 1. Location of measurement stations.

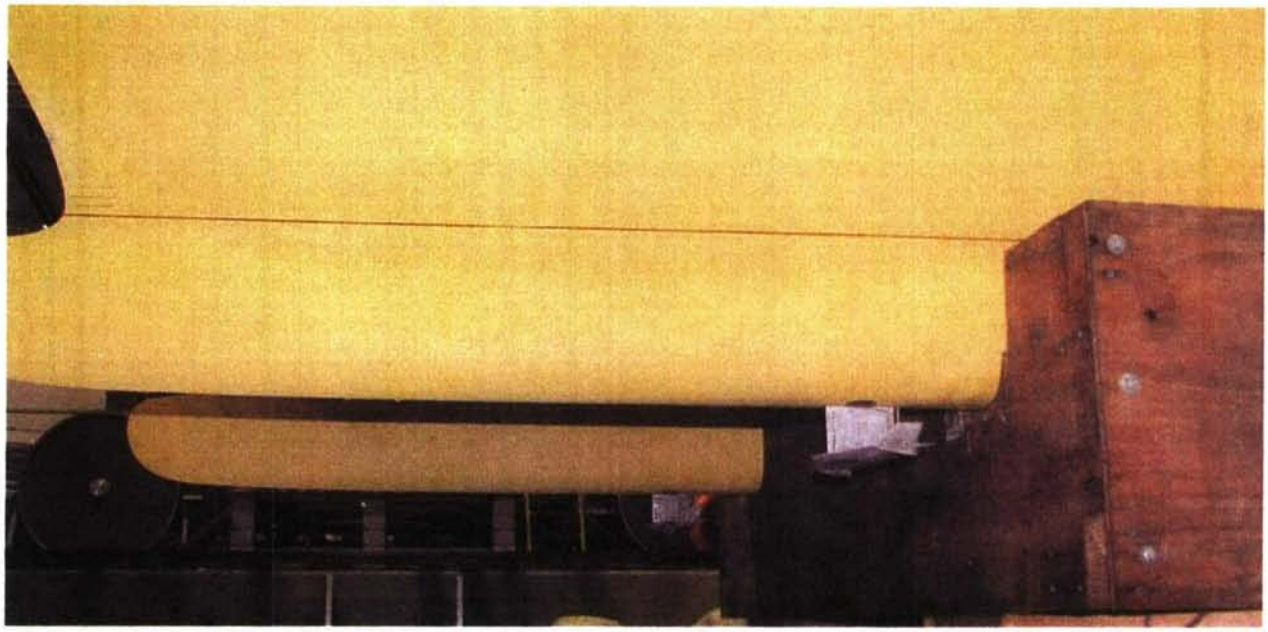

Fig. 2. T-foils.

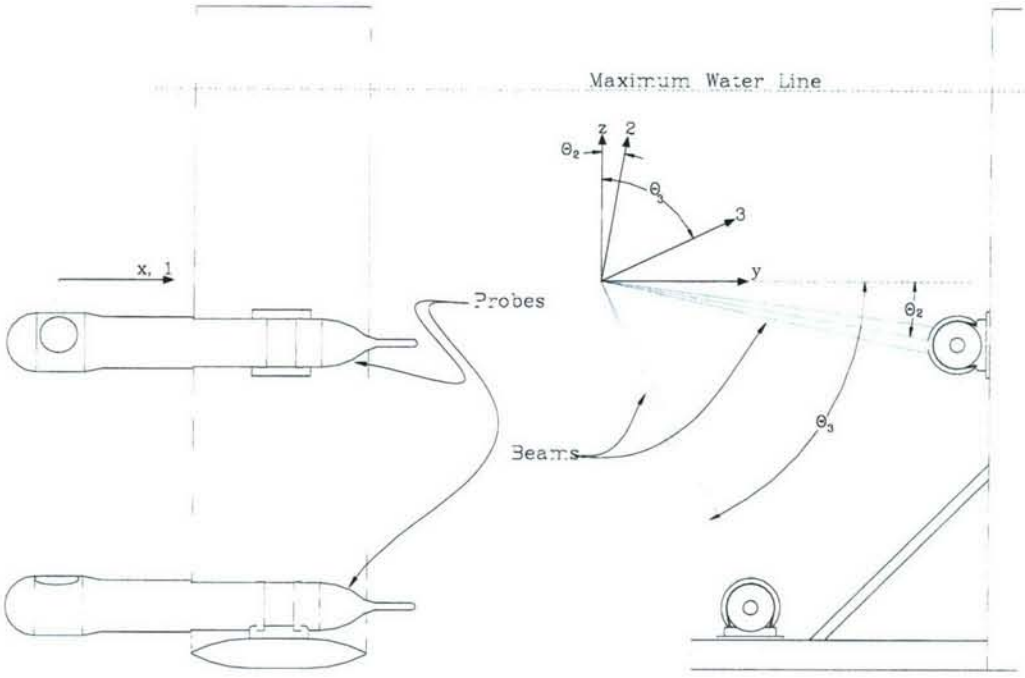

Fig. 3. Fiber-optic probes and strut.

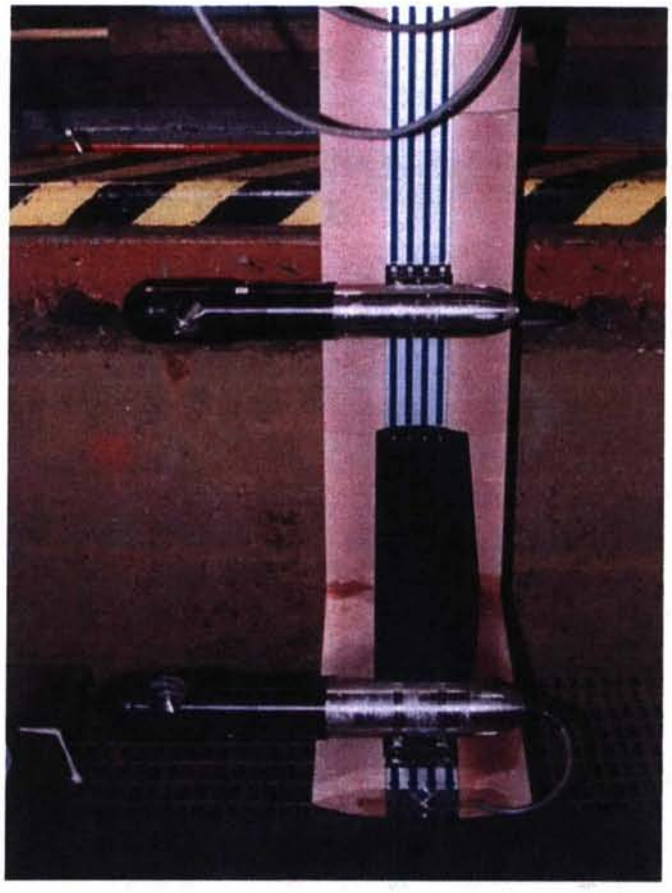

Fig. 4. Probes and strut in dry dock.

Fig. 5. Probes, strut, and hull.

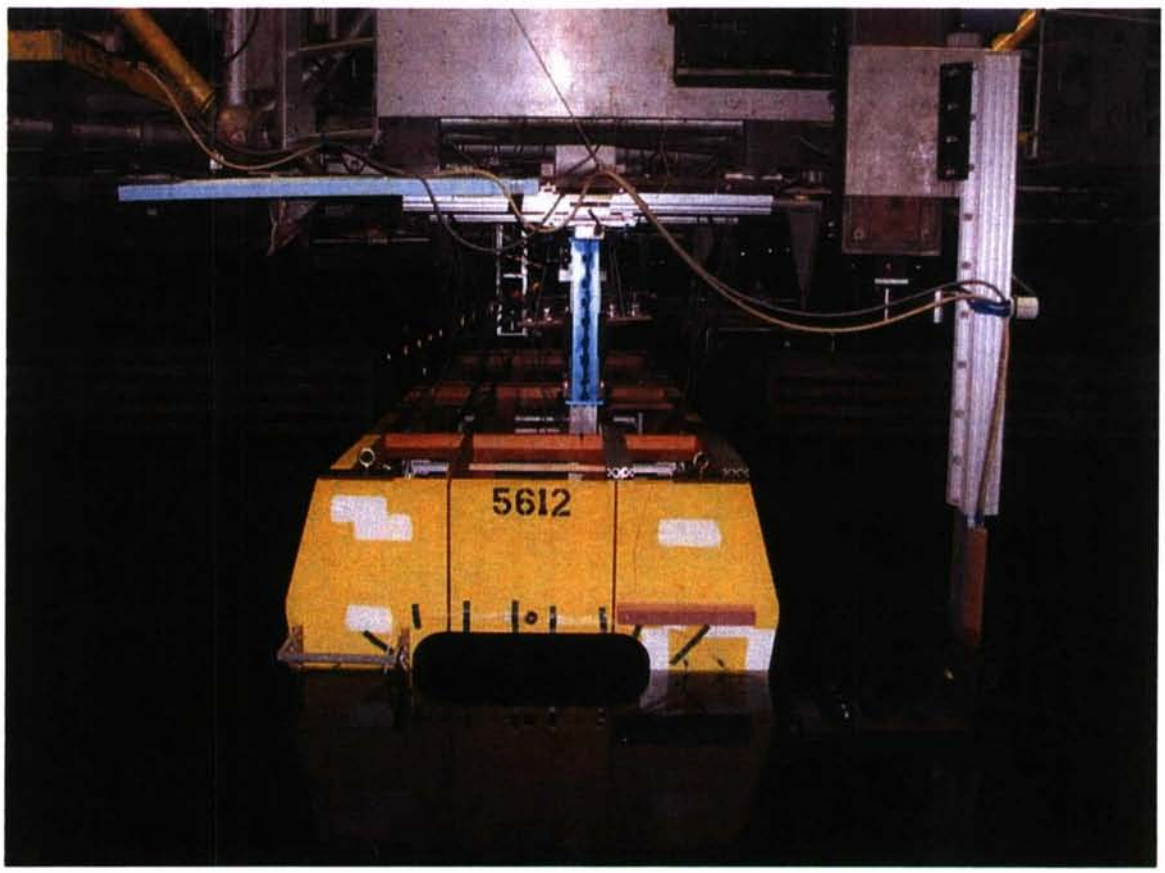

Fig. 6. LDV strut at station 1.

Fig. 7. LDV probe assembly, stations 3 and 6.

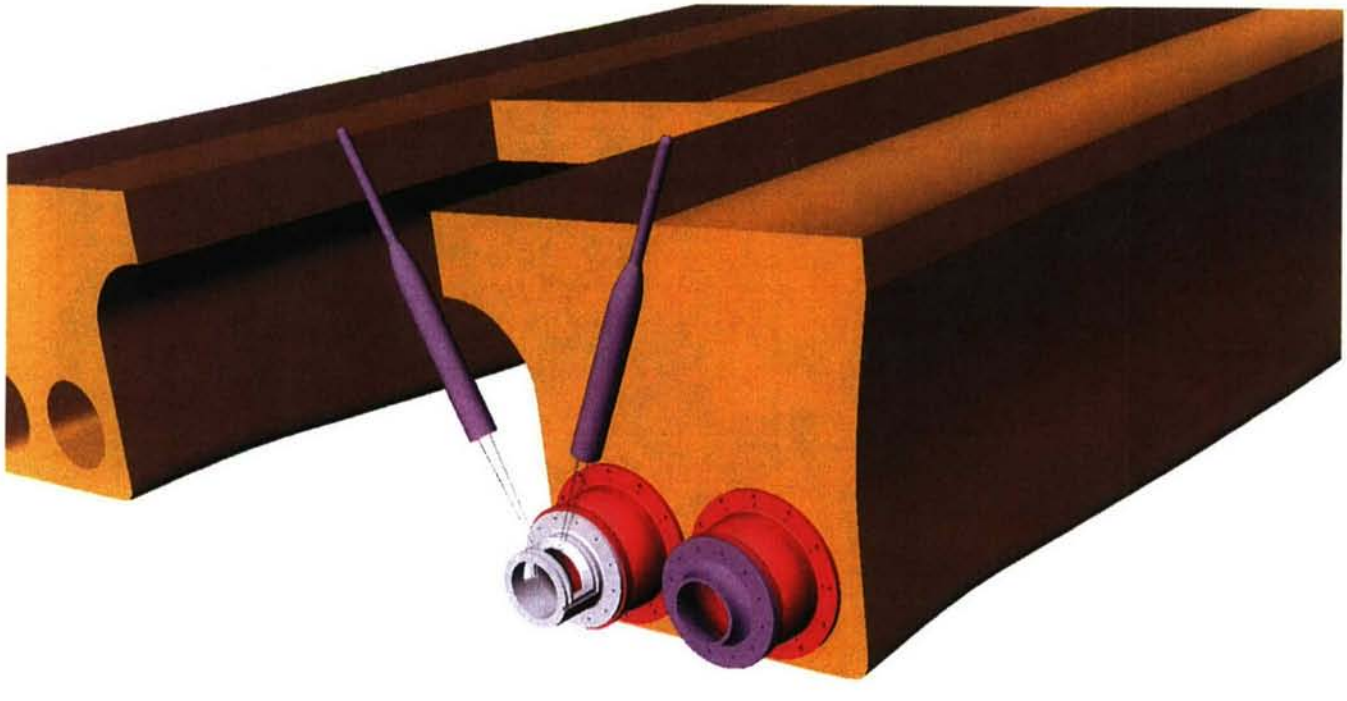

Fig. 8. Probe orientation at station 6.

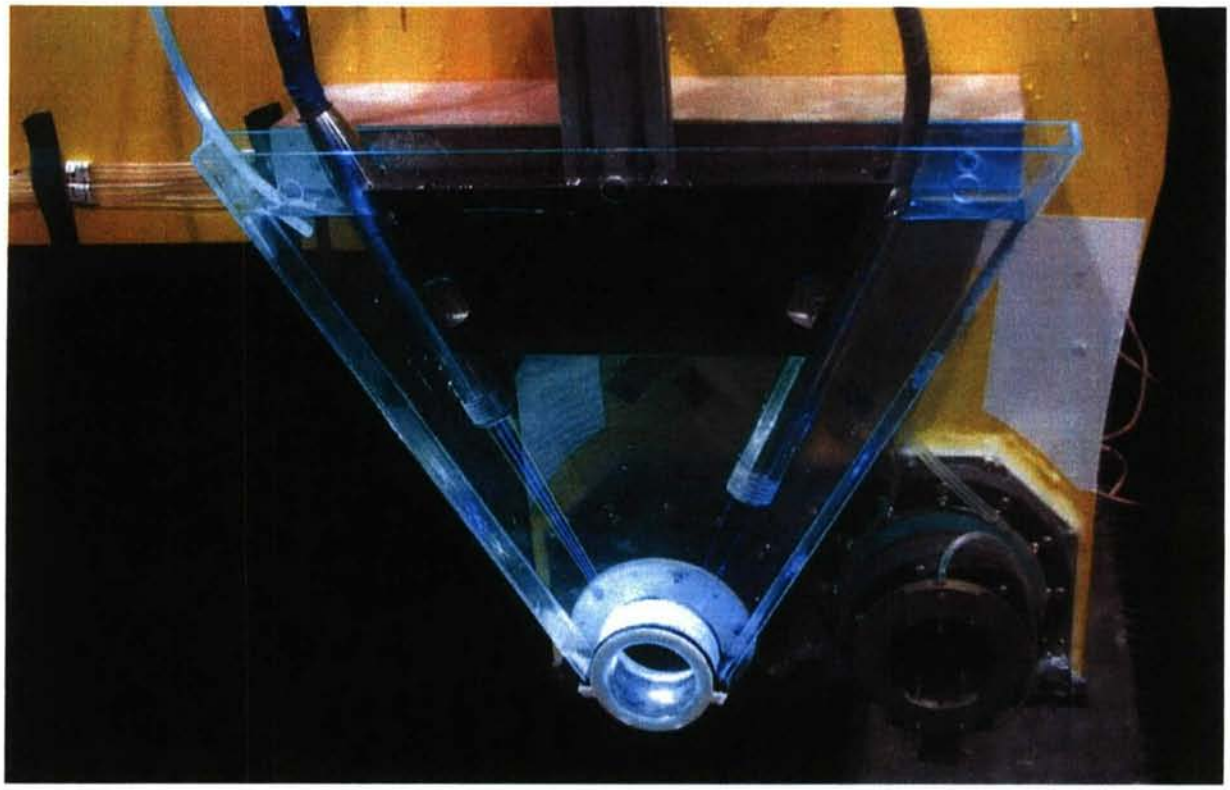

Fig. 9. Probes in water tank at station 6.
Green and blue beams on left (inboard) and violet beams on right (outboard).

Fig. 10. Waterjet operation underway at 40 kt., LDV at station 6.

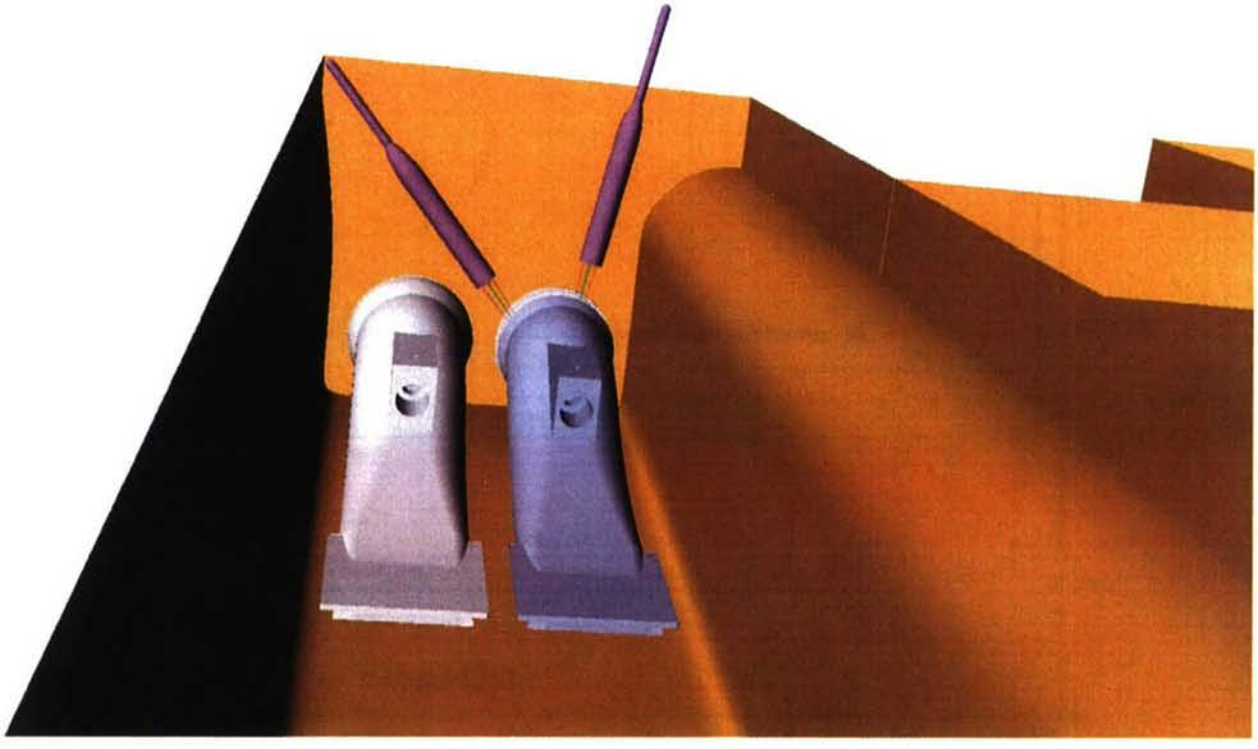

Fig. 11. Probe orientation at station 3.

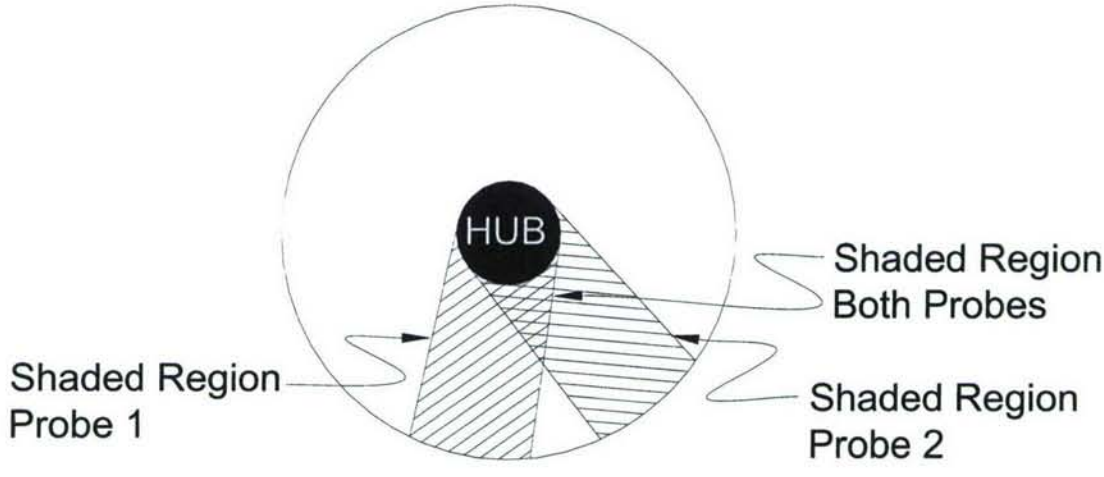

Fig. 12. Shadowed regions of flow, station 3.

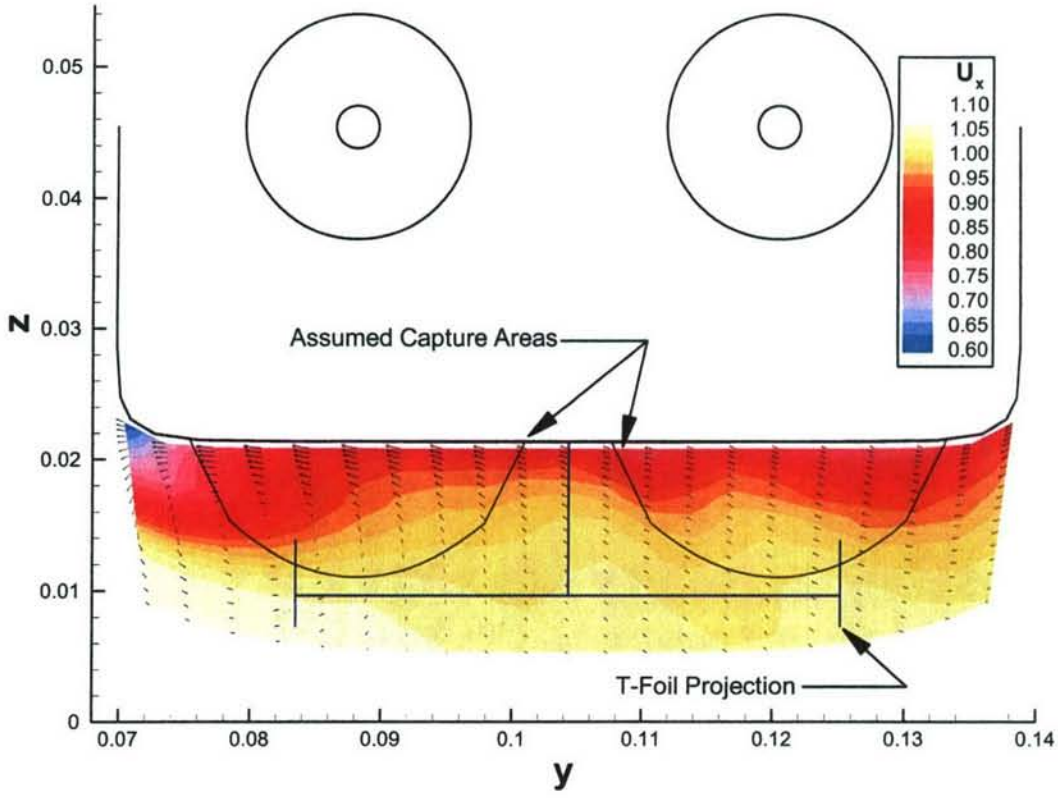

Fig. 13. Velocity at station 1, 25 kt., with outline of pump inflow area.

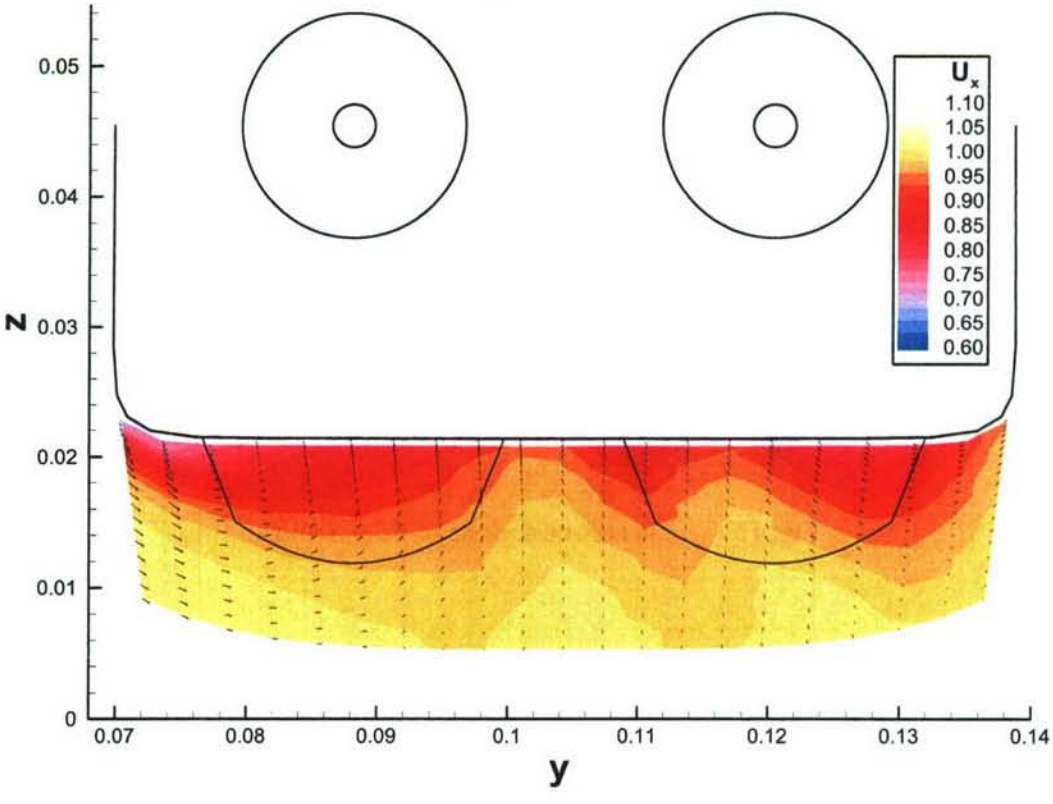

Fig. 14. Velocity at station 1, 40 kt., with outline of pump inflow area.

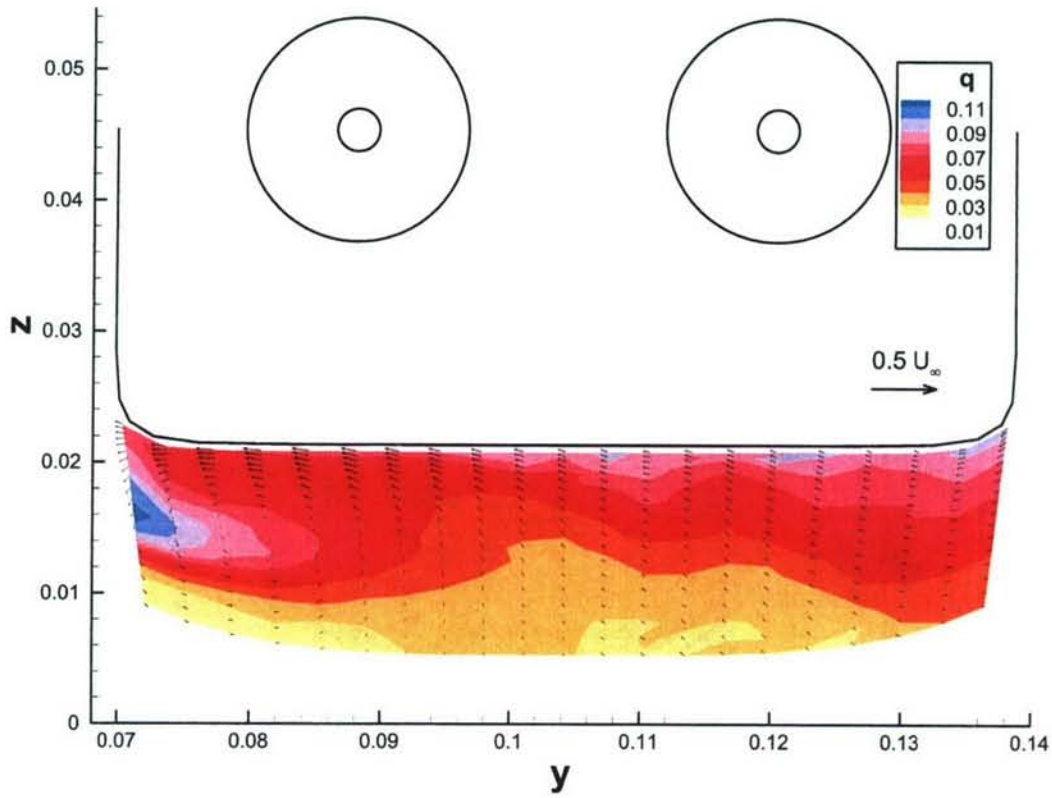

Fig. 15. RMS velocity at station 1, 25 kt..

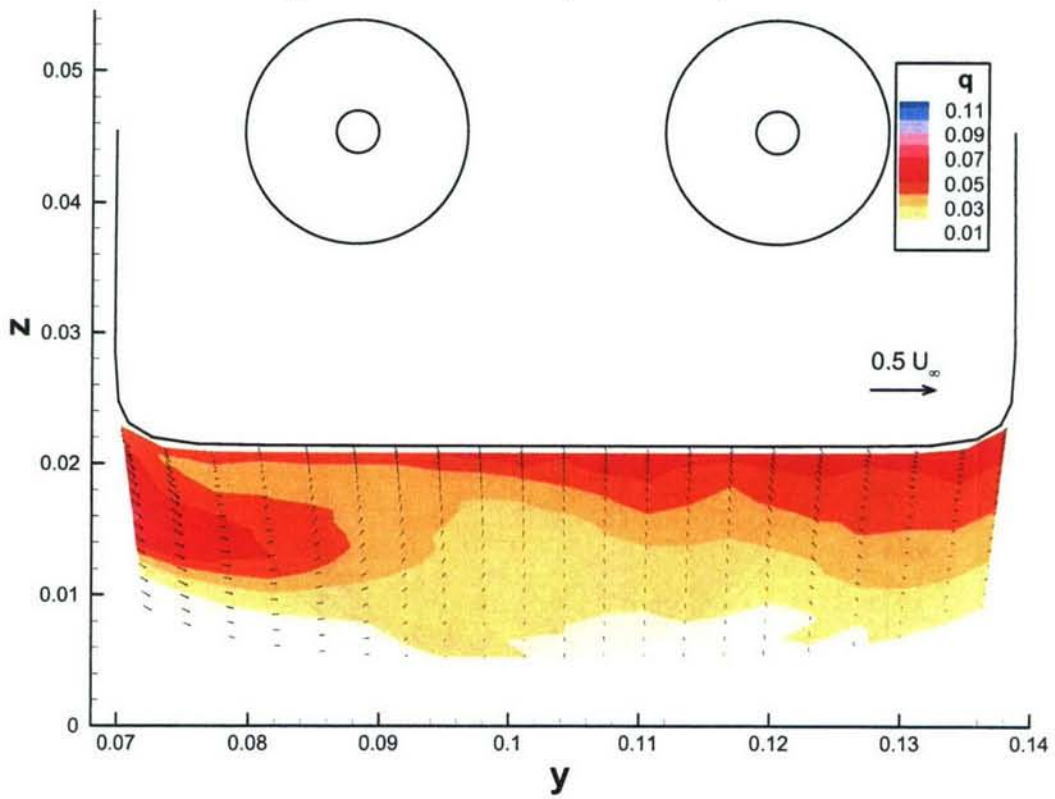

Fig. 16. RMS velocity at station 1, 40 kt..

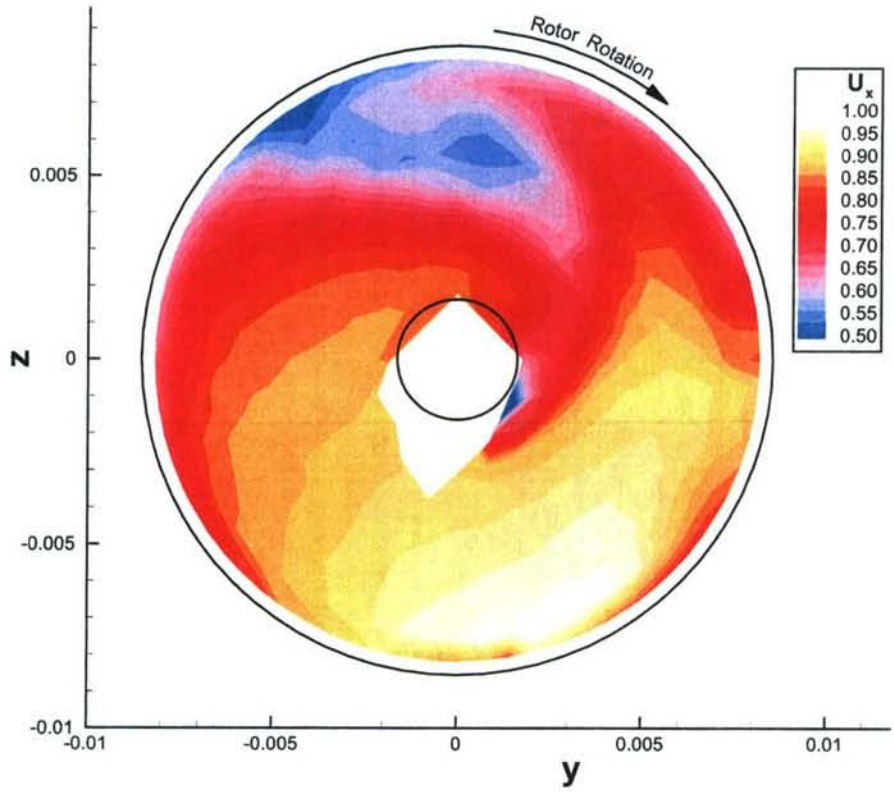

Fig. 17. Measured velocity at station 3, 25 kt..

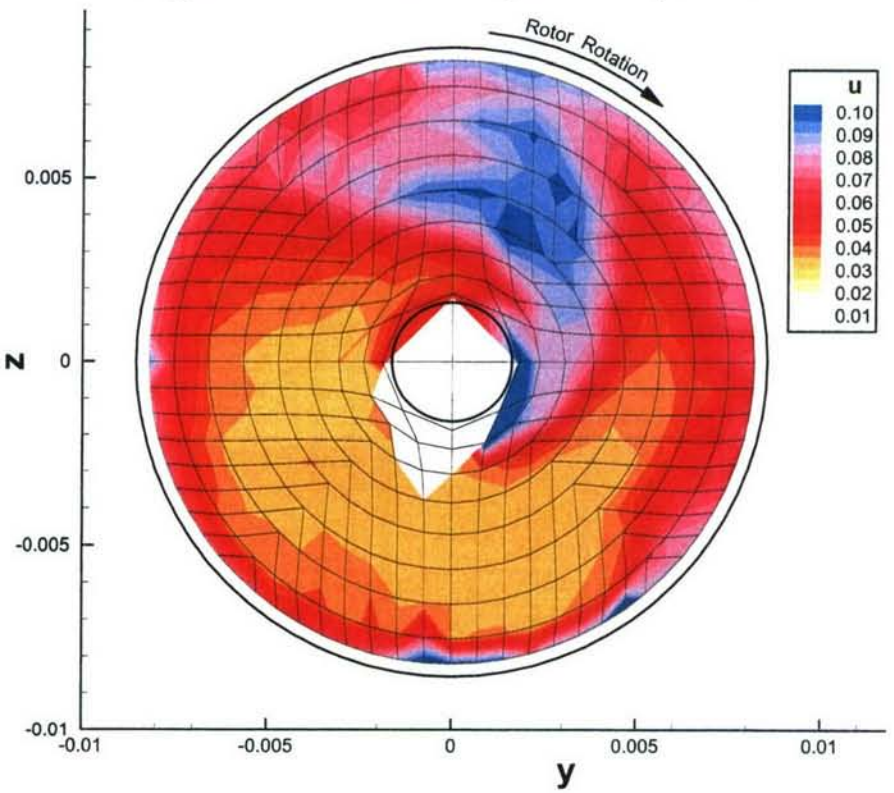

Fig. 18. RMS velocity at station 3, 25 kt..
Black lines show measurement grid.

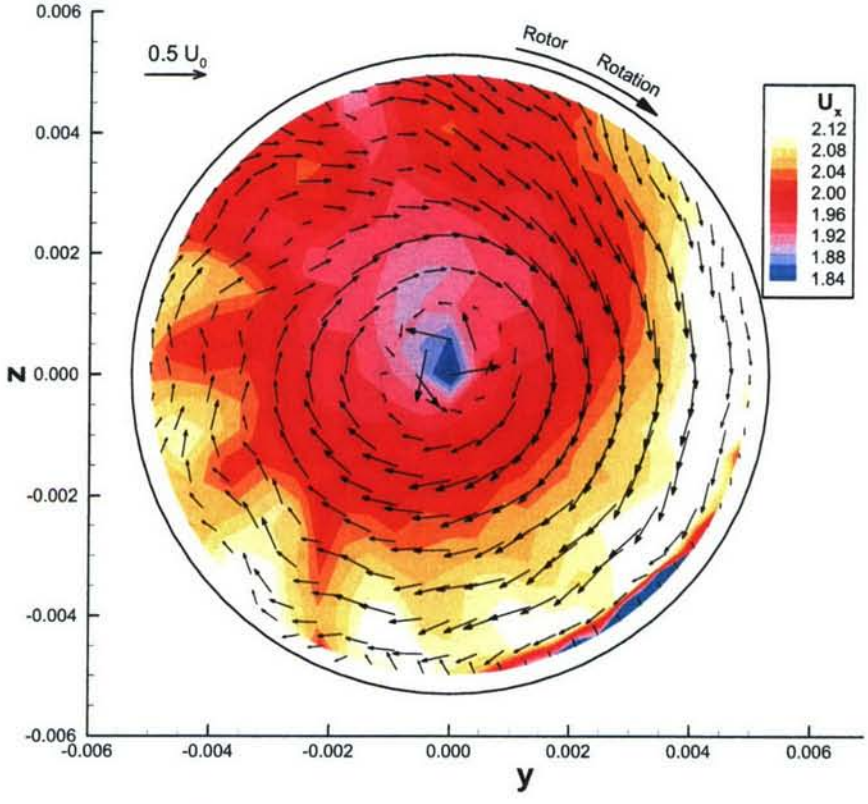

Fig. 19. Measured velocity at station 6, 25 kt..

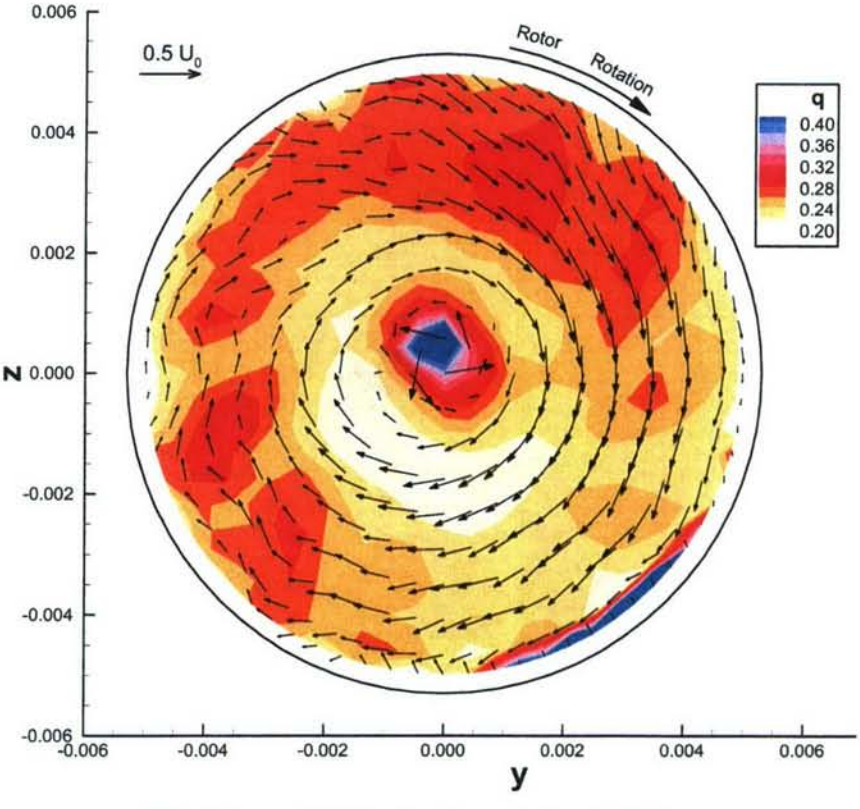

Fig. 20. RMS velocity at station 6, 25 kt..

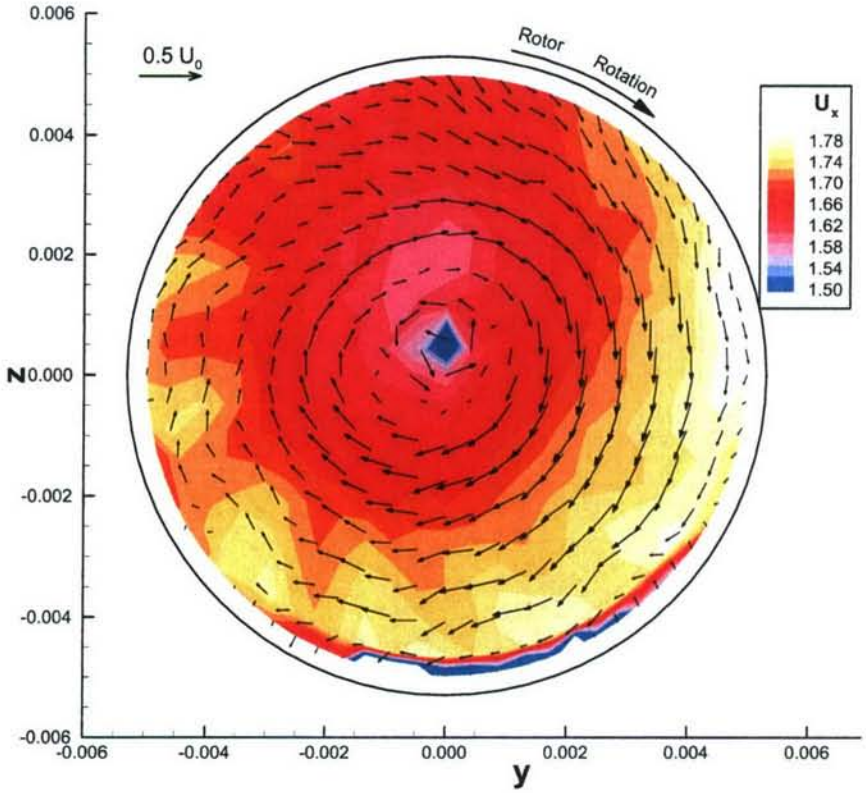

Fig. 21. Measured velocity at station 6, 40 kt..

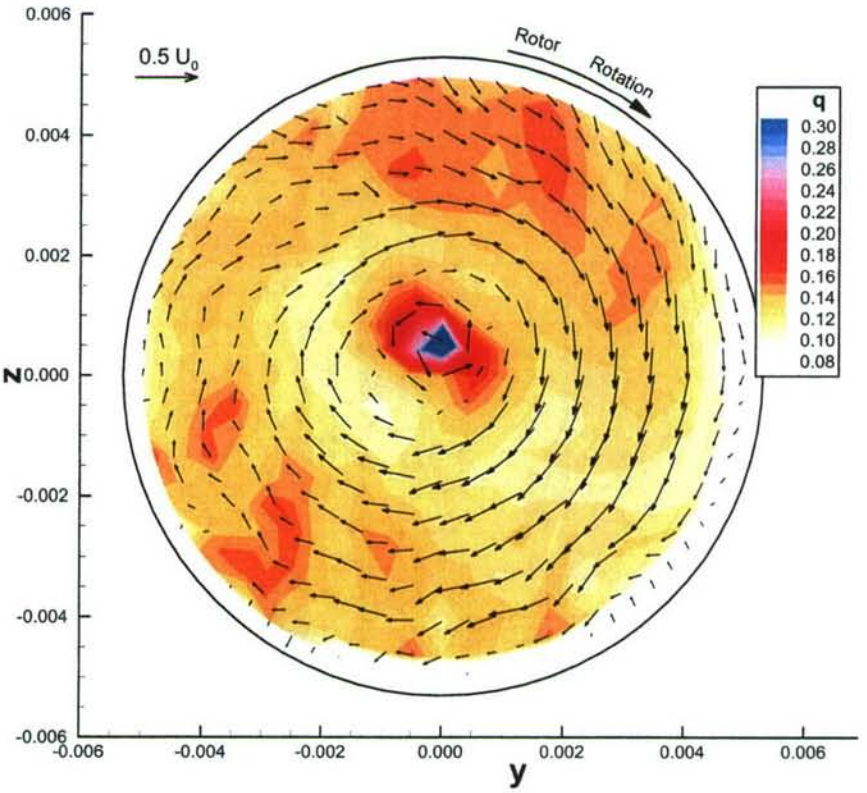

Fig. 22. RMS velocity at station 6, 40 kt..

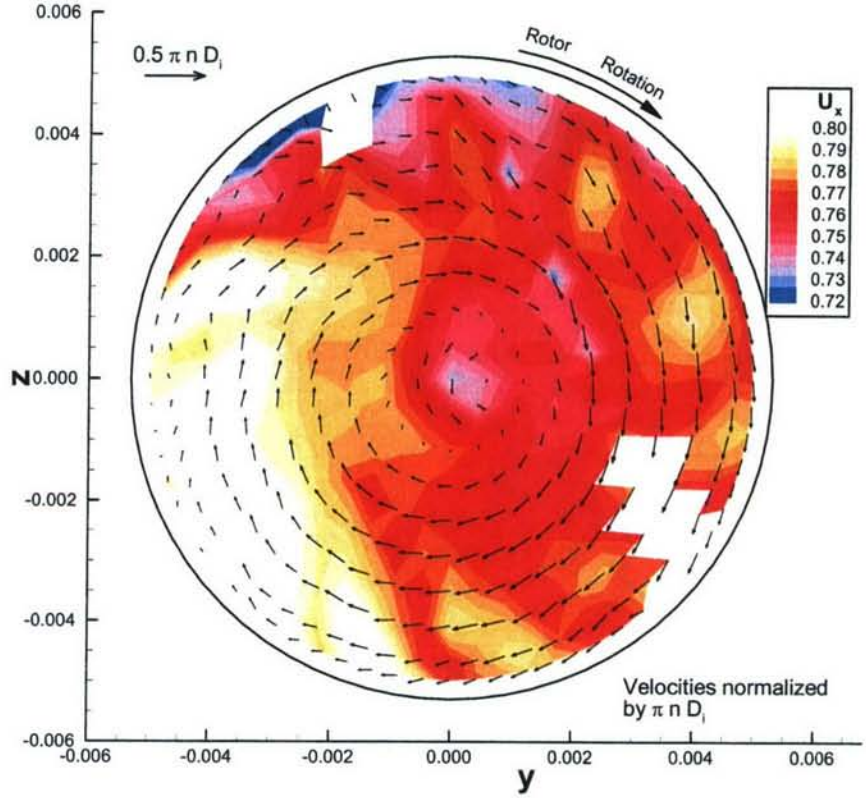

Fig. 23. Measured velocity at station 6, 1500 rpm bollard.

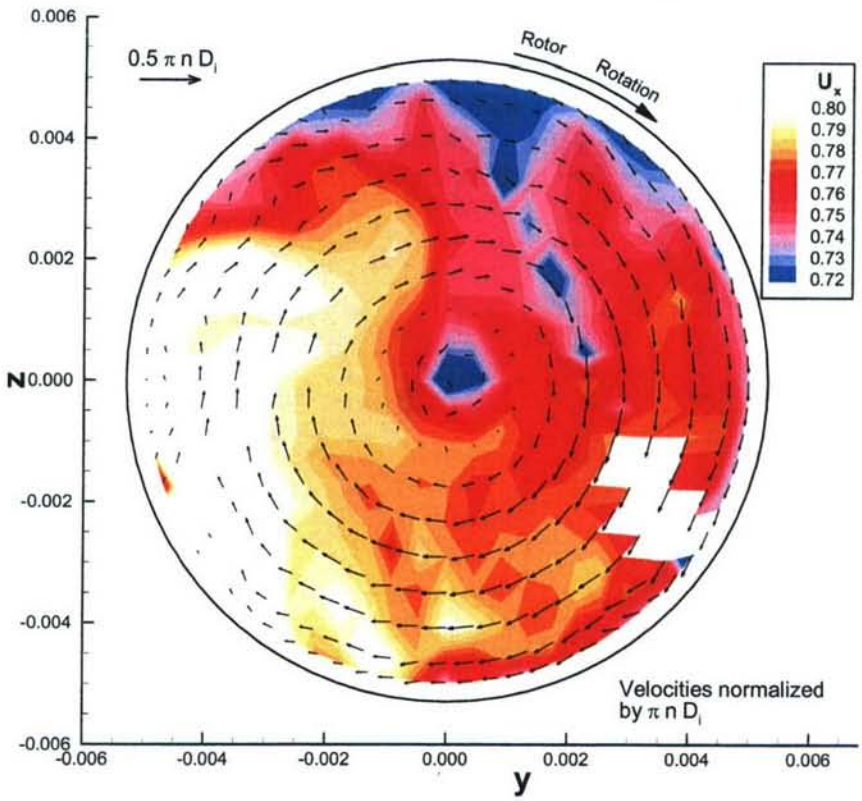

Fig. 24. Measured velocity at station 6, 2500 rpm bollard.

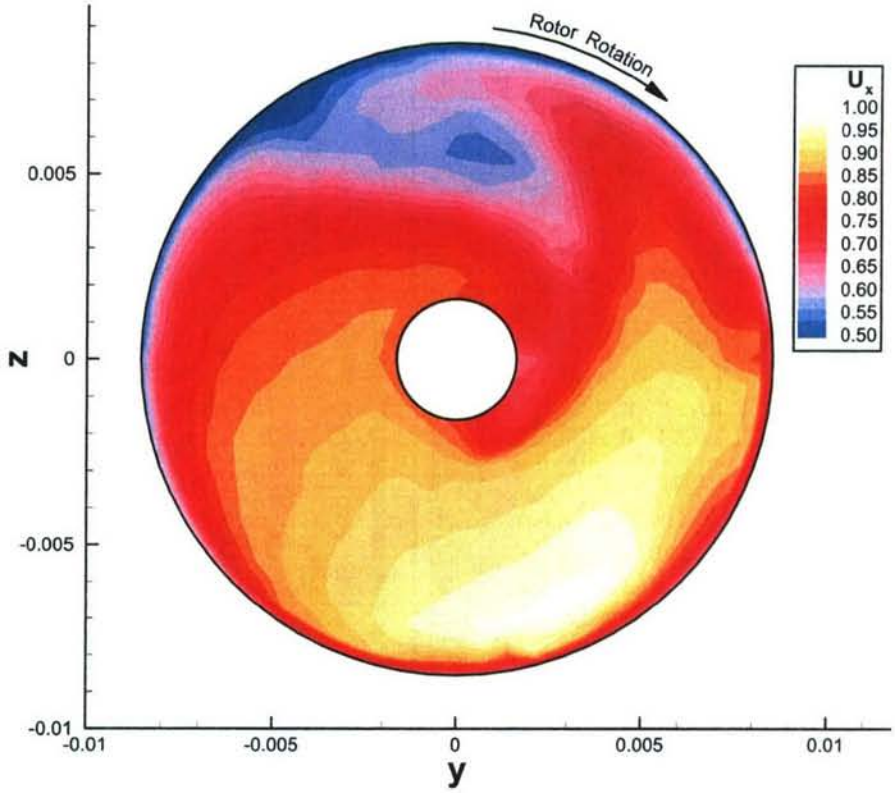

Fig. 25. Velocity field used for integrations at station 3, 25 kt.. Data near wall and shaft added.

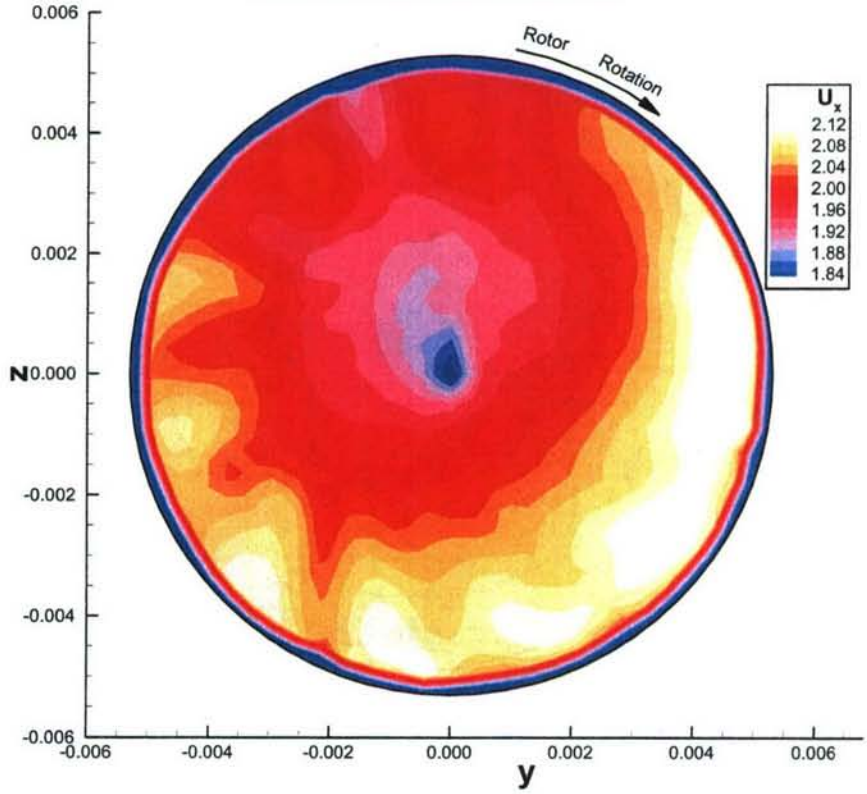

Fig. 26. Velocity field used for integrations at station 6, 25 kt..

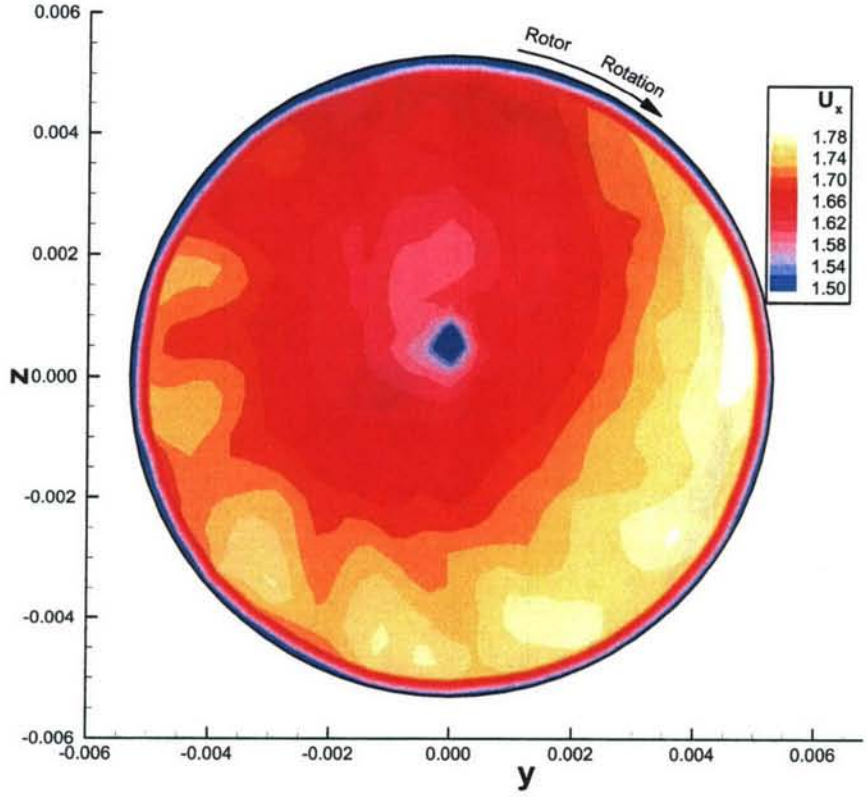

Fig. 27. Velocity field used for integrations at station 6, 40 kt..

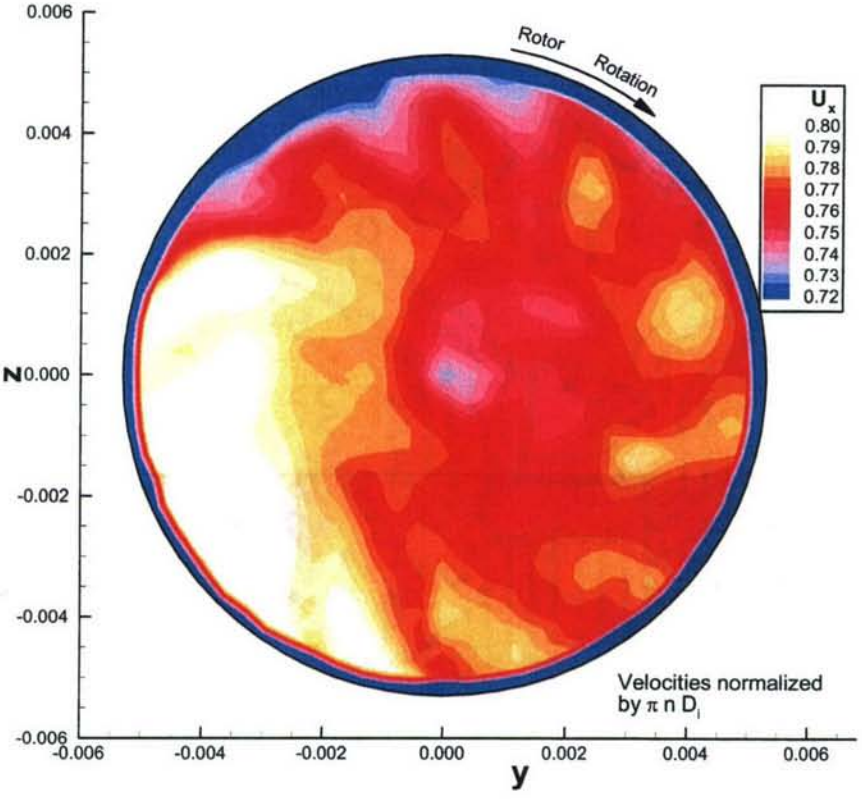

Fig. 28. Velocity field used for integrations at station 6, 1500 rpm bollard.

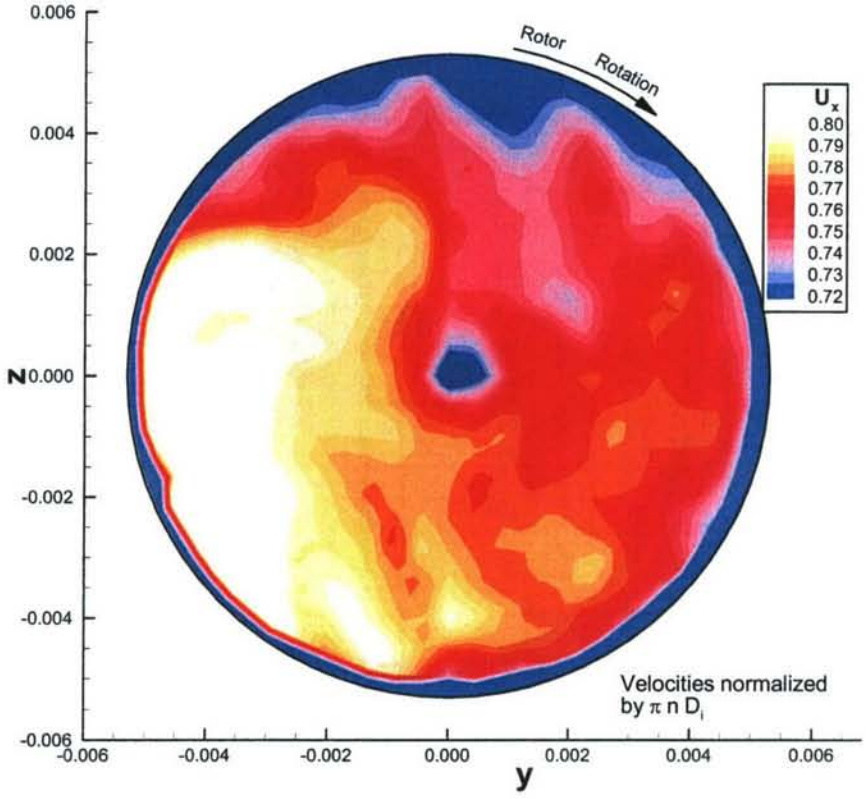

Fig. 29. Velocity field used for integrations at station 6, 1500 rpm bollard.

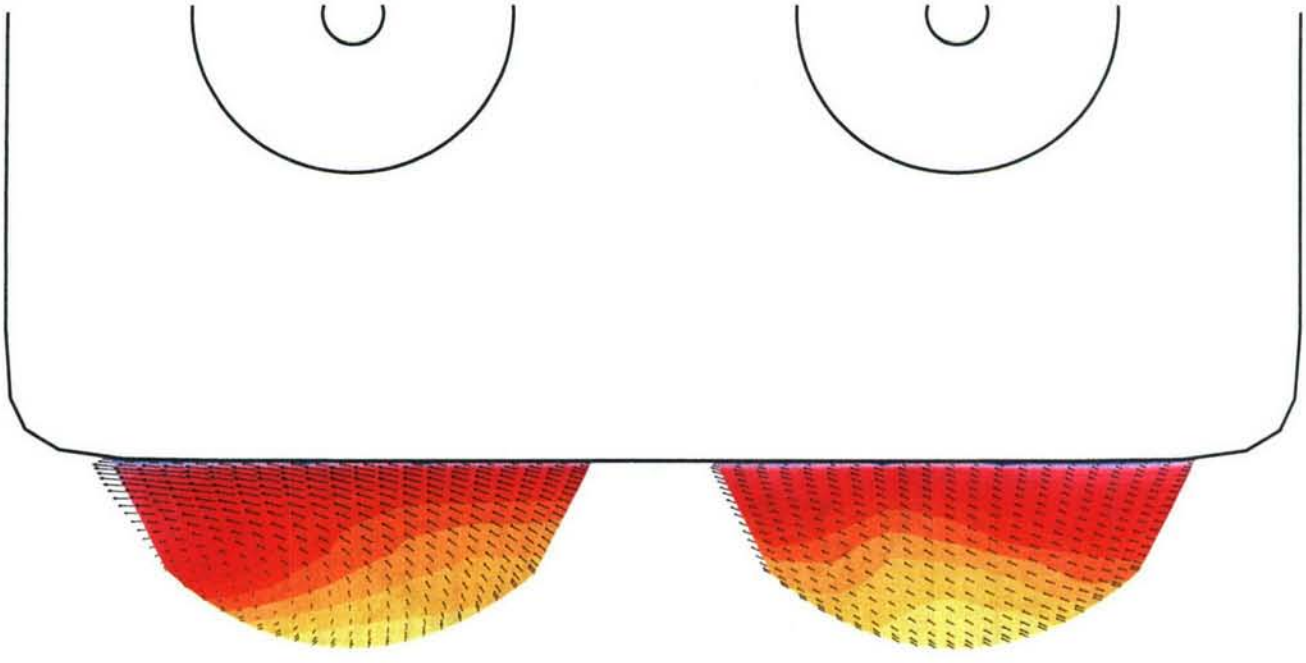

Fig. 30. Inflow areas at station 1, 25 kt..

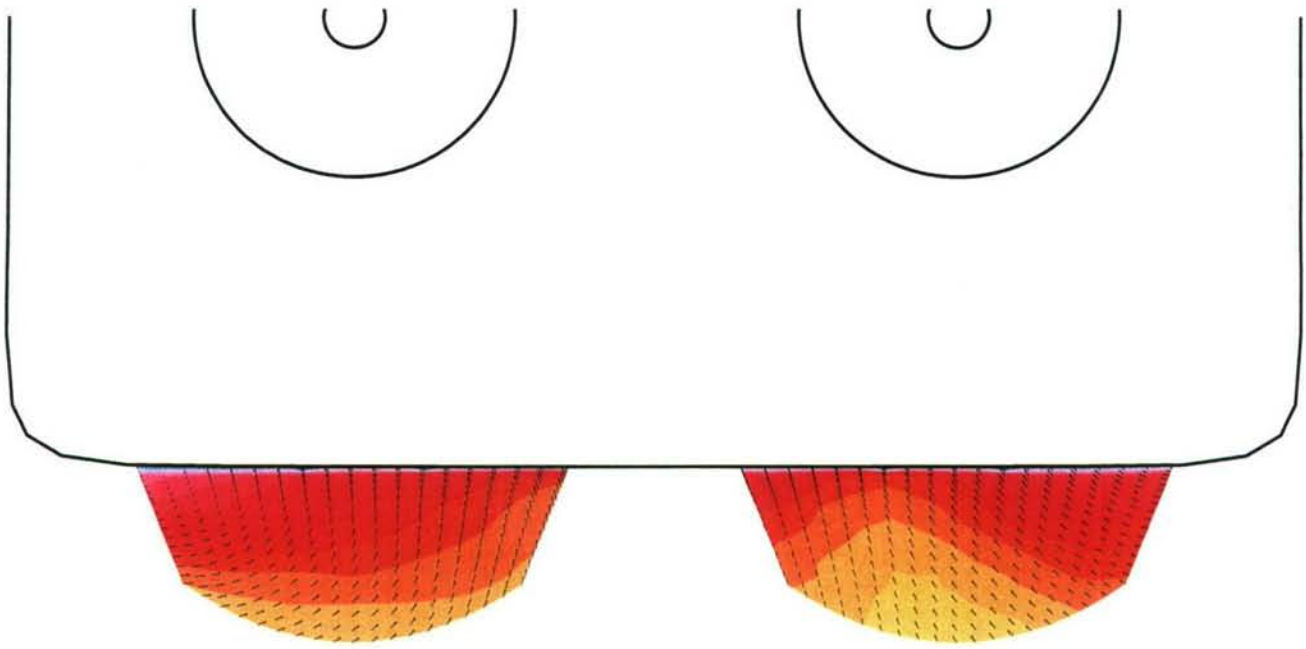

Fig. 31. Inflow areas at station 1, 40 kt..

(THIS PAGE INTENTIONALLY LEFT BLANK)

REFERENCES

[1] Chesnakas, C. J., "Velocity Measurements Inside the Pump of the Gulf Coast Waterjet Tow Tank Model 5600," NSWCCD-50-TR-2003/014, Naval Surface Warfare Center, Carderock Division, February 2003.

[2] Chesnakas, C. J., "3-D LDV Mapping of the Flow About a Waterjet-Powered Hull in a Tow Tank," 26th American Towing Tank Conference, Webb Institute, Glen Cove, New York, 23-24 July 2001.

[3] Scherer, J. O., Mutnick, I., and Chesnakas, C. J., "Towing Tank Tests of Model 5565-1 with Rolls Royce Naval Marine AWJ-21 Waterjet Propulsion," NSWCCD-50-TR-2002/028, Naval Surface Warfare Center, Carderock Division, July 2002.

(THIS PAGE INTENTIONALLY LEFT BLANK)

INITIAL DISTRIBUTION

Organization	Name	Copies
ONR		
033X	J. Harrison	1
033	K. Kim	1
033	P. Purtell	1
NAVSEA		
05D1	S. Wynn	1
05H	J. Schumann	1
PMS 325	W. Davison	1
	D. Liese	1
DTIC		2

CENTER DISTRIBUTION

Code	Name	Copies
001	J. Beach	1
002	J. Corrado	1
0021	J. Barkyoumb	1
2120	J. Offutt	1
2240	S. Fung	1
	C. Kennell	1
	G. Lamb	1
3452	NSWCCD Library	pdf only
5010	50 Admin. Office	w/o enc.
5030	S. Jessup	1
5050	A. Reed	1
5060	D. Walden	2
5200	D. Cusanelli	1
	W. Day	1
	S. Fisher	1
	G. Karafiath	1
	C. Lin	1
	B. Metcalf	1
5400	S. Black	1
	C. Chesnakas	5
	C. Dai	1
	M. Donnelly	1
	M. Ebert	1
	R. Etter	1
	J. Gorski	1
	S. Gowing	1
	J. Scherer	1
	Y. Shen	1
	M. Wilson	1
	Library	1
5500	T. Applebee	1
	A. Becnel	1
	D. Hayden	1
	J. Hoyt	1